Mean Sea Surface Model over the Sea of Japan and its Adjacent Ocean Determined from Multisatellite Altimeter Data, Tide Gauge Records and GNSS Data

Yupeng Niu[1], Jinyun Guo[1*], Jiajia Yuan[1], Chengcheng Zhu[1], Zhen Li[1]

[1]College of Geodesy and Geomatics, Shandong University of Science and Technology, Qingdao 266590, China

Corresponding author: Jinyun Guo (jinyunguo1@126.com)

Key Points:

- A new mean sea surface model with a grid of $1' \times 1'$ over the Sea of Japan and its adjacent ocean (named SJAO2020) is established
- The new altimetry data of HaiYang-2A, Jason-3 and Sentinel-3A have been used in establishing the SJAO2020 model
- Tide gauge stations and joint GNSS are used to improve the offshore accuracy of the SJAO2020 model.

Abstract

The mean sea surface (MSS) model is an important reference for the study of sea level change and charting data, and the coastal accuracy of the model has always been the focus of marine geophysics and oceanography. A new MSS model with a grid of $1' \times 1'$ over the Sea of Japan and its adjacent ocean (named SJAO2020) (25°N~50°N, 125°E~150°E), is established from a combination of 26 years of satellite altimeter data from a total of 12 different satellites and records of 24 tide gauge stations and joint GNSS data covering the period 1993-2018 by a 19-year moving average method. Different from the latest international MSS models CLS15 and DTU18, the data of the latest altimetry satellites HY-2A, Janson-3 and Sentinel-3A are also introduced, and tide gauge records as well as the joint GNSS data are used to correct the SSH within 10 km from the coastline by using the Gaussian inverse distance weighting method in the SJAO2020 model. By comparing with tide gauge records, satellite altimeter data and other models (DTU18, DTU15, CLS11 and WHU13), it can be demonstrated that the SJAO2020 model produces the smallest errors, and its offshore accuracy is relatively reliable.

1 Introduction

Mean sea surface (MSS) refers to the mean dynamic sea surface height relative to the reference ellipsoid at a certain period of time and includes two pieces of information: the mean dynamic topography (MDT) and the geoid (Andersen and Knudsen, 2009). MSS, as one of the key parameters of geodesy and oceanography, is widely used in ocean gravity calculations (zhu et al. 2019; 2020), water depth detection, the determination of geoid fluctuations, and the analysis of crustal deformation (Guo et al., 2016), which is a key issue in environmental science and earth science today.

Since 1973, Skylab, Geos-3, Seasat, Geosat, ERS-1, Topex/Poseidon (T/P), ERS-2, GFO, Jason-1, Envisat, ICEsat, Janson-2, Cryosat-2, HaiYang-2A (HY-2A), Saral, Janson-3, Sentinel-3A, Sentinel-3B and other altimeter satellites have been launched successively and have obtained large altimetry data sets, which have provided robust marine information resources for sea level research (Guo et al., 2015; Dufau et al., 2016). Multiple global or regional MSS models using various altimetry data were established by research scholars and institutions in related fields. In the early 1990s, Marsh et al. (1992) established an MSS model named MSS-9012 with $1/8^{\circ} \times 1/8^{\circ}$ spatial resolution between $62^{\circ}\,\mathrm{S} \sim 62^{\circ}\,\mathrm{N}$ based on Geos-3 and Seasat satellite data. With the decryption of Geosat data and the launch of other altimeter satellites, the temporal and spatial resolution of altimeter data has also been greatly improved, and the use of various altimeter data fusion techniques to establish the MSS model has entered an advanced stage. For example, the MSS models CLS_SHOM98.2 ($3.75' \times 3.75'$), CLS01 ($2' \times 2'$) (Hernandez and Schaeffer, 2001), CLS10 (Schaeffer et al., 2010), CLS11 (Schaeffer et al., 2012), and CLS15 ($1' \times 1'$) (Pujol et al., 2018) were established by the Center National d'Etudes Spatiales (CNES). DNSC08 ($1' \times 1'$), DTU10, DTU13 (Andersen et al., 2015), DTU15 (Andersen et al., 2016), and DTU18 (Andersen et al., 2018) MSS models have been published by the Technical University of Denmark (DTU). Wuhan University of China has established WHU2000 ($2' \times 2'$) (Jiang et al., 2002), WHU2009 (Jin et al., 2011), and WHU2013 (Jin et al., 2016).

CLS15 and DTU18 are the latest MSS models at present. The grid for both is $1' \times 1'$ and the coverage range of CLS15 is $80^{\circ}\,\mathrm{S} \sim 84^{\circ}\,\mathrm{N}$. DTU18 covers a range of $90^{\circ}\,\mathrm{S}$ to $90^{\circ}\,\mathrm{N}$ due to

the use of 8 years of synthetic aperture radar (SAR) and synthetic aperture radar interferometric (SARin) data from the Cryosat-2 satellites at the north and south poles. However, both CLS15 and DTU18 represent the mean sea surface height (MSSH) from 1993 to 2012, and the latest altimeter data of HY-2A, Janson-3 and Sentinel-3A were not added to the establishment of CLS15 and DTU18. These altimeter data will be used together with other altimeter data (i.e., T/P, Jason-1, Jason-2, Jason-3, ERS-1, ERS-2, Envisat, GFO, Cryosat-2 and Saral) covering the period 1993~2018 to establish a new MSS model in this study.

In the open ocean, the accuracy of satellite altimetry can reach the centimeter level. However, offshore altimeter echoes received by satellites are contaminated by the combined effects of land and geophysical environments. The data quality is greatly reduced (Guo et al., 2010; Yuan et al., 2020a), which severely restricts the offshore accuracy of MSS models. Tide gauge stations are located along the coastline, and the offshore accuracy of observations is high (Menéndez and Woodworth, 2010). The sea level observed by the tide gauge station is relative to a certain benchmark, so sea surface height (SSH) can be obtained from tide gauge records and joint GNSS data.

Therefore, a new MSS model over the Sea of Japan and its adjacent ocean (named SJAO2020) (25°N~50°N, 125°E~150°E) with a grid of $1' \times 1'$ is established using multisatellite altimeter data, tide gauge records and joint GNSS data by a 19-year moving average method (Yuan et al., 2020b). The process of establishing the SJAO2020 model has also been presented, including removal of the temporal oceanic variability of exact repeat mission (ERM) data and geodetic mission (GM) data, crossover adjustment, gridding and improving the offshore accuracy. This paper is organized as follows. Section 2 introduces the data sources and methodology. Section 3 presents the results, analysis and validations as well as the SJAO2020 models, and Section 4 offers the conclusion.

2 Data sources and methodology

2.1 Study area

The Sea of Japan is the largest semienclosed deep margin sea in the northwest Pacific. The Sea of Japan and its adjacent ocean (25°N~50°N, 125°E~150°E) are located at the intersection of the Eurasian plate, Pacific plate and Philippine sea plate (Bird, 2003) and exhibit a complicated submarine topography. Due to the collision between plates, there are many trenches in the study area, including the Ryukyu trench, the Izu-Bonin trench, the Japan trench, and the Kuril trench.

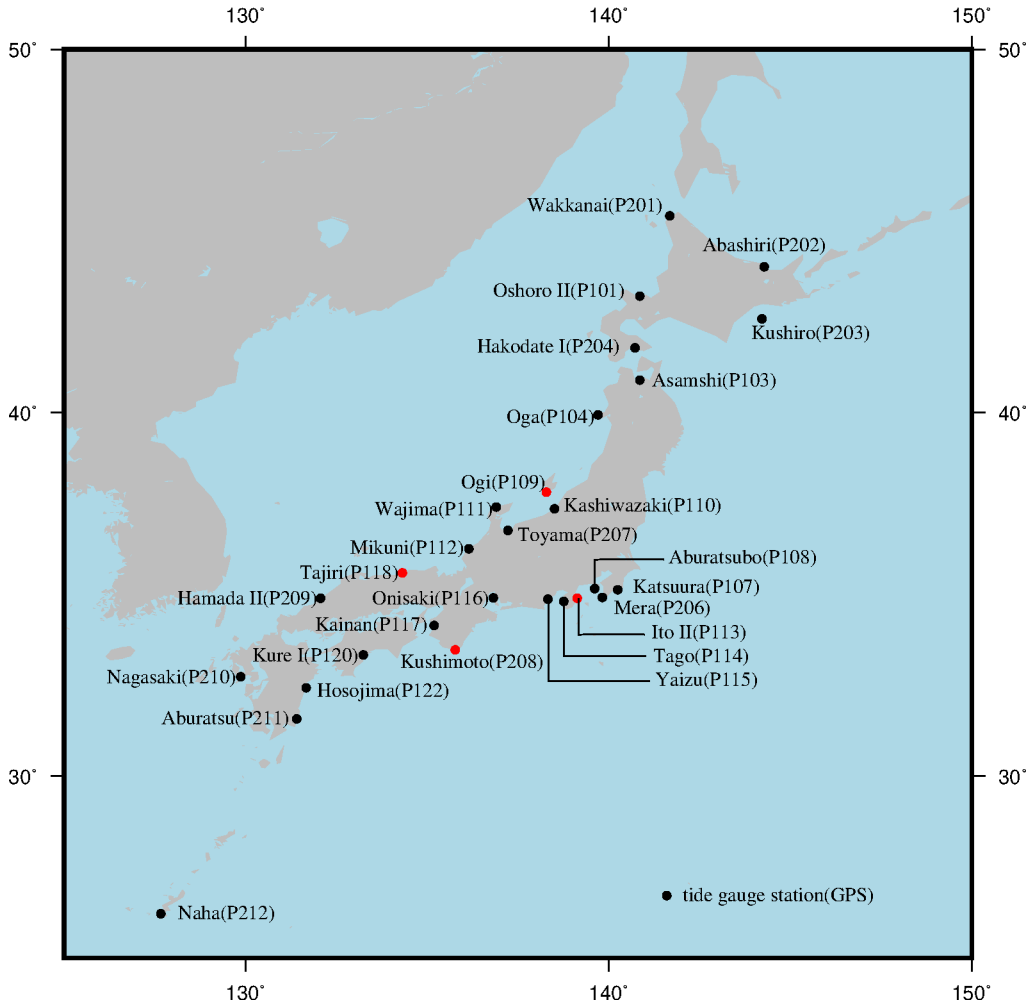

Figure 1. Research area and geographical distribution of tide gauge stations and joint GNSS

The coastline of Japan is very complicated, with a total length of approximately 33889 km. Because the sea level of the study area is affected by the Kuroshio current, internal circulation, El Niño and related dynamic mechanisms and thermal mechanisms, there are different long- and short-period components whose changes are more complex in the Sea of Japan and its adjacent ocean (Ishii et al., 2006).

2.2 Data sources

2.2.1 Satellite altimeter data

The satellite altimeter data used in this study are the Leve2+(L2P) SSH data published by Archiving Validation and Interpretation of Satellite Oceanographic Data (AVISO+) with a sampling frequency of 1 Hz (CNES, 2017). L2p data update the correction items of geophysical data records (GDR), control the data quality, and unify the reference ellipsoid and frame of each satellite datum. To establish a high-precision MSS model, the ERM data of the T/P, Jason-1, Jason-2, Jason-3, ERS-1, ERS-2, GFO, Envisat, HY-2A, Saral and Sentinel-3A satellites are used in this study. To improve the spatial resolution of the MSS model, the GM data of ERS-1/168, Jason-1/GM, Cryosat-2/LRM (Low resolution mode), Saral/DP (Drifting Phase) and HY-2A/GM satellites are also used in the model. The specific condition of each satellite is shown in Table 1.

Table 1 Satellite altimeter data used in this study

Satellite	Start and end date	cycles	Satellite	Start and end date	cycles
Topex/A	1992.12.31-2004.04.24	11-353	Envisat/B	2011.02.24-2012.02.19	100-111
Jason-1/A	2004.04.24-2008.10.19	11-249	SARAL	2013.03.14-2015.03.19	1-21
Jason-2/A	2008.10.19-2016.05.26	11-290	HY-2A	2013.04.12-2016.03.15	67-117
Jason-3/A	2016.05.26-2018.12.31	11-106	Sentinel-3A	2016.12.07-2019.01.02	12-39
Topex/B	2002.09.20-2005.09.24	369-479	ERS-1/168	1994.04.10-1995.03.21	30-40
Jason-1/B	2009.02.10-2012.02.15	262-372	Jason-1/GM	2012.05.07-2013.06.21	500-537
ERS-1/35	1992.11.27-1993.12.20 1995.03.24-1996.03.24	16-27 41-51	CryoSat-2/LRM	2011.01.28-2018.12.30	14-113
ERS-2	1995.12.31-2003.12.31	7-80	Saral/DP	2016.07.04-2018.12.31	100-125
GFO	2000.05.23-2008.05.16	45-215	HY-2A/GM	2016.03.30-2019.01.04	118-230
Envisat/A	2002.05.14-2010.05.31	6-89			

In Table 1, Topex/A, Jason-1/A, Jason-2/A, Jason-3 A and Envisat/A are the ERM data before orbital transfer of each satellite, while Topex/B, Jason-1/B and Envisat/B are the ERM data after orbital transfer of each satellite. All ERM data in Table 1 are selected from annual observations to minimize the temporal oceanic variability in the MSS.

The establishment of the MSS model used almost all satellite data on-orbit from 1993 to 2018, with a time span of 26 years in this study. The cycle of the lunar near-point orbit is 8.847-year, and the motion cycle of the ascending node of the lunar orbit is 18.621-year. To further eliminate the influence of the residual error of tide model error on the altimeter data, eight independent MSS models are established based on the 19-year interval in this study. Then the final MSS model is determined by calculating the average at each grid point of these eight MSS models. The offshore accuracy of the model will be improved later with the data of tide gauge stations and joint GNSS. The satellite altimeter data grouping is shown in Appendix A.

2.2.2 Tide gauge records

The accuracy of the MSS model established solely by satellite altimeter data is seriously affected due to the poor quality of the offshore altimeter data. Tide gauge records have long-term characteristics, relative stability and high offshore accuracy, so the offshore accuracy of satellite altimeter data can be corrected by tide gauge records. Thirty-five tide gauge stations along the coast of Japan on the Permanent Service for Mean Sea Level (PSMSL) have continuous annual data from 1993 to 2018. Only 28 tide gauge stations (Figure 1) have continuous GPS joint measurement data. Considering that the tide gauge records and GPS data are consistent in time and space, 24 tide gauge stations (the black solid circle in Figure 1) are selected to improve the offshore accuracy of the MSS model established only by

satellite altimeter data. The remaining 4 tide gauge stations (the red solid circle in Figure 1) are used for the validation of offshore accuracy. The annual tide gauge records are derived from revised local reference (RLR) sea level data released by the PSMSL (Holgate et al., 2013).

The missing values of the annual tide gauge records downloaded from the PSMSL are filled with extreme values of -99999. The missing rate of 28 tide gauge stations is 0.824%. The singular spectrum analysis (SSA) iterative interpolation method is used to complete the data (Shen et al., 2018; Hassani, 2007).

2.2.3 GPS data

The sea level measured by satellite is based on the reference ellipsoid, but the sea level observed by the tide gauge station is relative to a certain benchmark. The absolute SSH can be obtained from tide gauge records and joint GNSS data. The GPS data used were calculated by the University of La Rochelle (ULR) using GAMIT/GLOBK software, which can be downloaded from Systèmed' Observation duNiveau des Eaux Littorales (SONEL). The reference ellipsoid and the reference frame of GPS data are GRS80 and ITRF08. GPS time series data have made corresponding data corrections (Santamaría-Gómez et al., 2012; 2017) for earthquakes and other emergencies, which meet the requirements of this study.

2.3 Data processing method

2.3.1 Collinear adjustment of ERM data

After precise data editing and preprocessing, the SSH obtained by satellite altimetry has a higher accuracy. However, the instantaneous SSH still has large fluctuations and contains a large number of temporal oceanic variability signals. The collinear adjustment of the ERM data for each satellite can effectively eliminate the temporal oceanic variability of the SSH with a period shorter than the time span of the collinear tracks used and weaken the sea level anomalies (SLA) caused by large-scale ocean anomalies (such as El Niño and La Niña) in a specific period.

Because the satellite orbit is perturbed by some nonconservative forces, there is an offset of 1 ~ 2 km for the repetitive ground tracks in adjacent cycles. Sea level is a relatively smooth surface. The radar beam emitted by the altimeter satellite is a disc with a radius of 3 ~ 5 km after reaching sea level. In fact, the sea surface observations are also mean values on this surface. Therefore, this study simplifies the original collinear adjustment method to avoid the calculation of normal points. That is, collinear tracks that are relatively stable, in good observation conditions and with a large number of observations are selected as the reference track, and the observations of other periods are interpolated into the reference track to obtain the MSSH for a long time on average (Jin et al., 2016). To prevent outliers from appearing, when the difference in SSH between the reference track and other tracks is greater than 0.5 m, the points of other tracks are eliminated.

2.3.2 Temporal oceanic variability correction of GM data

Because the GM data do not have the characteristics of repeated cycles, it is impossible to use the method of collinear adjustment to eliminate the temporal oceanic variability effects and variables with random characteristics. Usually, the existing annual mean or monthly mean SLA models are used for temporal oceanic variability correction of GM data, but this will introduce the MSS information contained in the SLA model used. Since the T/P, Jason-1, Jason-2, and Janson-3 satellites are considered to have high measuring accuracy, the ground

track before orbital transfer of the four satellites is the same. They have been continuously observed for 26 years. The collinear MSSH obtained over such a long time should be closest to the true MSSH. Therefore, the track after the collinear adjustment of the four satellites T/P, Jason-1, Jason-2 and Janson-3 is used as the reference track. In the same observation period as the ERS-1/168, Jason-1/GM, CryoSat-2/LRM, SARAL/DP and HY-2A/GM satellites, the SLAs of the T/P, Jason-1, Jason-2 and Janson-3 data relative to the reference track are obtained. Then, the correction of SLA is interpolated using space distance weighted interpolation, realizing temporal oceanic variability correction of the original GM data.

Table 2 Corresponding data used for sea level variation correction of GM data

GM observations			Corresponding ERM data		
Satellite	Cycle	Observation period	Satellite	Cycle	Observation period
ERS-1	100-111	1994.04.10-1995.03.21	T/P	57-93	1994.0401-1995.04.03
CryoSat-2	14-113	2011.01.28-2018.12.30	Jason-2	94-303	2011.01.20-2016.10.02
			Jason-3	1-106	2016.02.17-2019.01.03
Jason-1	500-537	2012.05.07-2013.06.21	Jason-2	140-183	2012.04.20-2013.06.03
HY-2A	118-230	2016.03.30-2019.01.04	Jason-2	284-303	2016.03.18-2016.10.02
			Jason-3	4-107	2016.03.18-2019.01.13
SARAL	100	2016.07.04-2018.12.31	Jason-2	294-303	2016.06.25-2016.10.02
			Jason-3	14-106	2016.06.25-2019.10.02

2.3.3 Crossover adjustment

Long-wavelength sea level changes of satellite observations can be weakened by collinear adjustment and temporal oceanic variability correction, such as the radial orbit error and the temporal variability of SSH. However, the residual radial orbit error, short-wavelength signal of temporal oceanic variability and geophysical correction residuals are still the main influences on the determination of MSS. The crossover adjustment can further weaken the residual radial orbit error of satellites, and realize the improvement of observations with lower orbit accuracy by satellite data with higher orbit accuracy.

The traditional crossover adjustment generally uses the radial orbit error as the main error source to establish the adjustment model, and the solution process is too complicated. With the improvement of orbit technology, the radial orbit error of the new generation of satellite altimeter data has been effectively controlled. The current satellite altimeter data are dynamic interferences in many aspects. The combined effects of these disturbances are very complex. In this study, the posteriori compensation method is used (Huang, 2007). First, the conditional adjustment is used to adjust the crossover observation equation, and then a new error model is used to filter and predict the SSH along the altimetry track.

When the condition adjustment is carried out, the SSH observation at any point along the track is expressed as

$$h = h_0 + \Delta \tag{1}$$

Where h is the SSH observation, h_0 is the true value of h, and Δ is the observation error.

According to equation (1), at the crossover point of ascending track *i* and descending track *j*, the conditional equation can be established as

$$v_{ij}^{a} - v_{ij}^{d} = h_{ij}^{a} - h_{ij}^{d} = d_{ij} \tag{2}$$

Where d_{ij} is the SSH difference at the crossover point. For a track network with multiple crossover points, the matrix form of the crossover point condition equation can be written as

$$\boldsymbol{AV} + \boldsymbol{W} = 0 \tag{3}$$

where $\boldsymbol{A}$ is the coefficient matrix, which consists of 1 and -1; $\boldsymbol{V}$ is the correction vector of the observation error; and $\boldsymbol{W}$ is the difference vector of crossover points. The least square solution of equation (3) is

$$\boldsymbol{V} = -\boldsymbol{P}^{-1}\boldsymbol{A}^{T}\left(\boldsymbol{A}\boldsymbol{P}^{-1}\boldsymbol{A}^{T}\right)^{-1}\boldsymbol{W} \tag{4}$$

The corresponding cofactor matrix is

$$\boldsymbol{Q}_{V} = \boldsymbol{P}^{-1}\boldsymbol{A}^{T}\left(\boldsymbol{A}\boldsymbol{P}^{-1}\boldsymbol{A}^{T}\right)^{-1}\boldsymbol{A}\boldsymbol{P}^{-1} \tag{5}$$

where $\boldsymbol{P}$ is the weight matrix of the observation vectors. Assuming that each observation point on the altimetry track is an independent observation, we can derive

$$v_{ij}^{a} = p_{ij}^{d} d_{ij} / \left(p_{ij}^{a} + p_{ij}^{d}\right) \tag{6}$$

$$v_{ij}^{d} = -p_{ij}^{a} d_{ij} / \left(p_{ij}^{a} + p_{ij}^{d}\right) \tag{7}$$

where p_{ij}^{a} and p_{ij}^{d} represent the weight factors of observations at the crossover point of the ascending track *i* and descending track *j*.

The comprehensive effect of residual error changes is very complicated, including parts that change linearly and parts that change periodically, and more are parts that have more complicated changes. According to the research results of Wagner (1985) and Rummel (1993), the traditional error model is extended to the following mixed polynomial model with the observed time as the independent variable (Huang et al., 2007). It can be expressed as

$$f(t) = a_0 + a_1\left(t - T_0\right) + \cdots + a_n\left(t - T_0\right)^{n} + \sum_{i=1}^{m}\left(b_i \cos iw\left(t - T_0\right) + c_i \sin iw\left(t - T_0\right)\right) \tag{8}$$

where t is the observed time; $a_i\left(i = 0, 1, 2, \cdots, n\right)$, b_i and $c_i\left(i = 1, 2, \cdots, m\right)$ are undetermined coefficients; and *w* represents the angular frequency corresponding to the periodic change of the error, which can generally be expressed as

$$w = 2\pi / \left(T_1 - T_0\right) \tag{9}$$

where T_0 and T_1 represent the corresponding observation times at the beginning and end of the altimetry track, respectively.

After the crossover adjustment is completed, for each altimetry track, according to the

error model of equation (8), the error equation can be expressed as

$$v = f(t) + \delta \tag{10}$$

where δ is the observation noise. The matrix form of equation (14) is

$$V = BX - l \tag{11}$$

where $\boldsymbol{l}$ is the correction vector of the observation of SSH at the crossover point; $\boldsymbol{B}$ is a matrix of known coefficients; $\boldsymbol{X}$ is the required parameter vector of the error model; and $\boldsymbol{V}$ is the vector of $\boldsymbol{l}$ corrections. The least squares solution of adjusted observation equations for equation (11) is

$$X = \left(B^T P_l B \right)^{-1} B^T P_l l \tag{12}$$

where P_l is the weighted matrix of $\boldsymbol{l}$. Substituting the error model coefficients obtained by equation (12) into equation (8), the corresponding system deviation correction can be completed according to the observation time of each altimetry track point.

2.3.4 Least-squares collocation technique for gridding

Most of the orbital errors and residual temporal oceanic variability errors are weakened by the intersection adjustment. However, the differences at the crossover point after adjustment indicate that there is still residual error, especially the GM observations. The least-squares collocation (LSC) technique for gridding can effectively use the prior information of the observations to solve the optimal estimate of the interpolated value. That is, different weights are given according to the residual error after adjustment to reduce the impact on the accuracy of the SSH.

When using the LSC to grid the SSH, the signal must have a zero-mean characteristic. Therefore, the reference MSS model must first be removed from the satellite altimeter data after crossover adjustment. In this study, the CLS15 MSS model in the L2p data product is selected as the reference MSS model. Then, the residual SSH is gridded. Before gridding, the average of the residual SSH should be subtracted to satisfy the zero-mean characteristic. Finally, the MSS model is obtained by adding the grid value to the average and restoring the removed reference MSS model.

Suppose a certain observation vector $\boldsymbol{y}$ contains a zero mean signal $\boldsymbol{t}$ and a zero mean noise vector $\boldsymbol{v}$ and is expressed as

$$y = t + v \tag{13}$$

where the self-covariance matrices of $\boldsymbol{t}$ and $\boldsymbol{v}$ are C_{tt} and C_{vv}, respectively; there is no correlation between $\boldsymbol{t}$ and $\boldsymbol{v}$, that is, $C_{tv} = 0$. Using the LSC technique, for any zero mean signal $\boldsymbol{s}$ in the data distribution, the fitted value is

$$\hat{s} = C_{st} \left(C_{tt} + C_{vv} \right)^{-1} y \tag{14}$$

where C_{st} is the cross-covariance between signal $\boldsymbol{s}$ and signal $\boldsymbol{t}$, and again, there is no correlation between $\boldsymbol{s}$ and $\boldsymbol{v}$. If the self-covariance C_{ss} of the signal s is known, the estimation error of s can be expressed as

$$E_{ss} = C_{ss} - C_{st}\left(C_{tt} + C_{ww}\right)^{-1} C_{st}^{T} \tag{15}$$

When the fitting point and the observation point coincide, the observation point is considered to have no error, that is, $C_{st}=C_{tt}=C_{ss}$, $C_{ww}=0$. From equations (14) and (15), the estimated value $\hat{s}=t$ and the error $E_{ss}=0$ satisfy the general interpolation method. Therefore, when the cross-covariance between the a priori information and the signal as well as the error is accurately known, LSC can effectively use the a priori information of the observations to obtain accurate interpolation values.

Because the satellite altimeter observations are very large and the data around each network point are densely distributed, they are insensitive to the accuracy of the covariance function when determining the MSSH of each network point (Yi, 1995). Therefore, a second-order Markov process is used to describe the one-dimensional covariance function (Small, 1992). The process can be expressed as

$$\operatorname{cov}(d) = C_0(1 + d/\alpha)e^{-d/\alpha} \tag{16}$$

where d is the distance between the observation point and the grid point; C_0 is the local variance parameter, which can be expressed by the variance of all observations in the local range involved in the grid. $\alpha=0.595\xi$, ξ is the relevant length, and the value is 70 km (Basic and Rapp, 1992). The single-satellite crossover differences accuracy of $1/\sqrt{2}$ times after the crossover adjustment is introduced into the LSC as the noise of the corresponding satellite data.

2.3.5 The method for improving the offshore accuracy of the model

First, inverse barometer correction is performed on the tide gauge records after preprocessing. Then, the SSH based on the GRS80 reference ellipsoid is obtained by adding the corrected tide gauge records and the joint GPS data. Through the reference ellipsoid and reference frame conversion, the SSH of the tide gauge records is converted to the T/P reference ellipsoid and frame. Finally, the 19-year moving average method is used to obtain the SSH at each tide gauge station.

In this study, the SSH difference between the tide gauge records and the model grid points within 10 km of 24 tide gauge stations is obtained. The Gaussian inverse distance weighting method is used to correct the SSH of the offshore grid points of the MSS model established only by multisource satellites. The correction value Δh of each grid point is

$$\Delta h = (H_{tide} - H_{ssh}) \times p \tag{17}$$

where H_{tide} is the tide gauge SSH; H_{ssh} is the SSH at the grid point of the MSS model; and p is a weighting factor weighted by the Gaussian inverse distance, which can be expressed as

$$p = e^{-\frac{d^2}{\alpha^2}} \tag{18}$$

where α is the Gaussian distance smoothing factor, which is 10 km in this study, and *d* is the spherical distance from the grid point to the tide gauge station. The calculation equation is

$$R = a \times \sqrt{1-e^2} \,/\, (1 - e^2 \times \sin^2((y_t + y_s)/2)) \tag{19}$$

$$d = 2 \times R \times \sqrt{\sin^2(\Delta y) + \cos(y_t) \times \cos(y_s) \times \sin^2(\Delta x)} \tag{20}$$

Where a is the long semiaxis of the T/P reference ellipsoid; y_t and x_t are the latitude and longitude of the tide gauge station; y_s and x_s are the latitude and longitude of the grid point; $\Delta y = (y_t - y_s)/2$; and $\Delta x = (x_t - x_s)/2$.

Finally, in the study area, the correction of the offshore (10 km from the coastline) grid points of the MSS model is realized by the spline interpolation method (Smith and Wessel, 1990) of adjustable tensor continuous curvature in GMT.

3 Results and analysis

3.1 Establishment of the MSS model based on satellite altimetry

3.1.1 Correction of temporal oceanic variability

To validate the effect of correction of temporal oceanic variability, the crossover differences of the altimetry satellite data before and after temporal oceanic variability correction were separately counted. The statistical results are shown in Table 3.

Table 3 The crossover difference of SSH in ERM data and GM data before and after temporal oceanic variability correction

Altimetric satellite	Before temporal oceanic variability correction (m)			Before temporal oceanic variability correction (m)		
	Mean	STD	RMS	Mean	STD	RMS
Topex/A+Jason-1/A+ Jason-2/A+ Jason-3/A	-0.0003	0.1971	0.1971	0.0018	0.0179	0.0179
Topex/B+Jason-1/B	0.0122	0.1598	0.1602	-0.0023	0.0291	0.0292
ERS-1	-0.0095	0.1983	0.1985	0.0017	0.0452	0.0453
ERS-2	-0.0090	0.2216	0.2185	-0.0049	0.0815	0.0816
GFO	0.0164	0.1818	0.1825	0.0034	0.0277	0.0279
Envisat/A	0.0191	0.1898	0.1908	-0.0024	0.0258	0.0260
Envisat/B	0.0065	0.1692	0.1693	0.0023	0.0632	0.0632
Saral	-0.0094	0.1842	0.1844	0.0015	0.0444	0.0444
HaiYang-2A	0.0012	0.1867	0.1867	0.0005	0.0328	0.0328
Sentinel-3A	0.0064	0.1801	0.1802	-0.0030	0.0293	0.0295

ERS-1/168	-0.0016	0.1883	0.1883	-0.0080	0.1202	0.1204
Jason-1/GM	0.0282	0.1882	0.1861	-0.0016	0.1120	0.1120
Cryosat-2/LRM	-0.0189	0.1866	0.1876	0.0002	0.1109	0.1109
Saral/DP	0.0011	0.1851	0.1851	0.0010	0.1128	0.1128
HY-2A/GM	0.0016	0.2021	0.2021	-0.0010	0..1235	0.1235

Table 3 shows that the accuracy of the ERM data is greatly improved after collinear adjustment. This shows that the temporal oceanic variability signal has a great influence on the MSS. Collinear processing can weaken the effect of temporal oceanic variability on ERM data and improve (better than 10 cm) the calculation accuracy of the SSH. The T/P series, as the spatial-temporal fundamental, has the highest accuracy of crossover differences. According to Table 2, temporal oceanic variability correction is performed on the GM data. The effect of temporal oceanic variability correction is shown in Table 3, in which the crossover difference is improved by approximately 7 cm.

3.1.2 Reduction of the influence of radial orbit errors

The residual radial orbit error of the satellite can be effectively reduced by the self-crossover adjustment of the satellite. Satellite observations with high orbit accuracy improve satellite observations with low orbit accuracy by combining all satellite data with the crossover adjustment. The combined effects of the above radial orbit errors and other errors have been further eliminated, realizing the unity and coordination of the combined processing of multiple satellite altimeter data.

Table 4 The crossover difference after crossover adjustment

Altimetry satellite	After crossover adjustment		
	Mean	STD	RMS
Topex/A+Jason-1/A+Jason-2/A+ Jason-3/A	0.0003	0.0068	0.0068
Topex/B+Jason-1/B	-0.0015	0.0245	0.0245
ERS-1	0.0004	0.0246	0.0246
ERS-2	-0.0003	0.0444	0.0444
GFO	0.0008	0.0155	0.0155
Envisat/A	-0.0002	0.0159	0.0159
Envisat/B	0.0015	0.0372	0.0372
Saral	0.0003	0.0270	0.0270
HaiYang-2A	0.0003	0.0266	0.0266
Sentinel-3A	0.0003	0.0257	0.0257
ERS-1/168	0.0002	0.0985	0.0985
Jason-1/GM	-0.0007	0.0942	0.0942
Cryosat-2/LRM	0.0001	0.0917	0.0917
Saral/DP	0.0004	0.0951	0.0951

HY-2A/GM	-0.0009	0.1021	0.1021
all satellite	0.0001	0.0811	0.0811

It can be seen from Tables 3 and 4 that after the self-crossover adjustment between the satellites, the STD of the crossover difference of SSH in ERM data is at the level of 1~4 cm and the GM data is approximately 9 cm, which effectively reduces the residual radial orbit errors of each satellite. The STD of the crossover difference after the joint crossover adjustment of each satellite is 0.0811 m, realizing the improvement of satellite observations with high accuracy to the satellite observations with low accuracy. The T/P series data are used as the reference data, and the STD of the self-crossover difference is 0.0068 m, which is much smaller than that of other satellites. Therefore, it is still in a dominant position in the joint crossover adjustment, and the coordination between multiple satellites is achieved while the benchmark is basically unchanged.

3.1.3 Establishment of model

The LSC method is a statistical estimation method based on the observation covariance information, taking full account of the statistical correlation between the data, and the smoothing function is higher than Shepard, continuous curvature tension spline and other analytical methods, so it is more suitable to grid satellite altimeter along-track data after crossover adjustment. The MSS model over the Sea of Japan and its adjacent ocean was determined from multisatellite altimeter data (named SJAO2020A) by taking the average of these 8 MSS models.

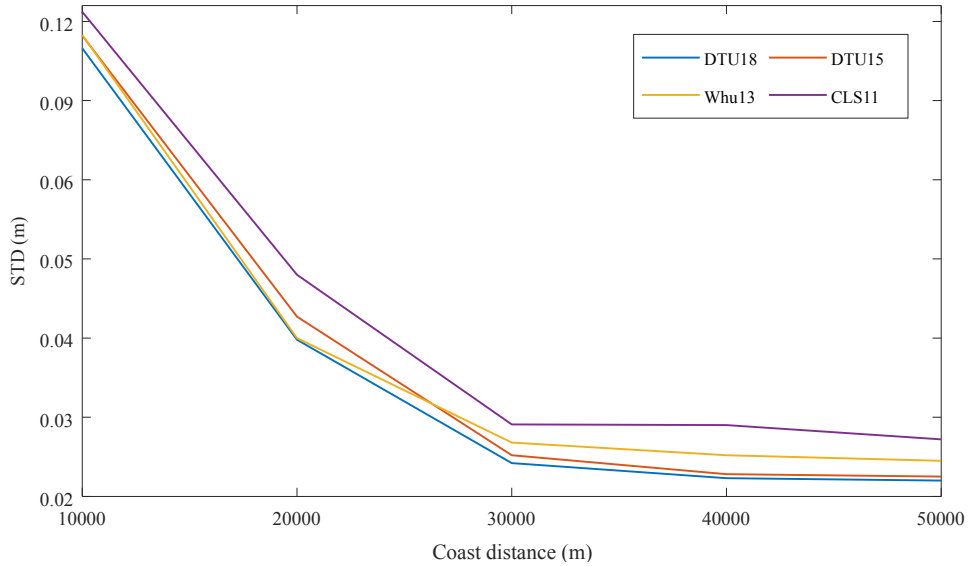

Figure 2 STDs of the SJAO2020A modol compared to different global MSS models

Figure 2 shows the STD of the difference between the SJAO2020A and DTU18, DTU15, Whu13 and CLS11 models within 10 km, 10-20 km, 20-30 km, 30-40 km and 40-50 km from the coastline. Within 5 groups of distances, the STD of the difference between SJAO2020A and DTU18 is always the smallest, and the largest is that of CLS11. The satellite altimeter data used in the establishment of the DTU18 model are the closest to SJAO2020A regardless of the type or amount of data. The CLS11 model was established using only the satellite data from 1993 to 2009, and the GM data were only used from the ERS-1 satellite from 1994 to 1995. The STD of the difference between SJAO2020A and the other four models decreases with increasing distance from the coastline, and the largest decrease is

within the range of 10~20 km. After 40 km, the STD is relatively stable, at approximately 0.025 m, indicating that the accuracy of SJAO2020A is relatively stable and reliable. However, these MSS models are very different in offshore areas, which is caused by the low offshore accuracy of satellite altimeter data. Therefore, improving the offshore accuracy of SSH is extremely important for improving the overall accuracy of the MSS model. In this study, the offshore accuracy of SJAO2020A was improved using 24 tide gauge stations and joint GPS around the Japanese coastline.

3.2 Improvement of model offshore accuracy

3.2.1 Determining the scope of offshore correction

The echo waveforms of altimetry satellites in the open sea are all standard waveforms, and the satellite observation accuracy is high. In offshore areas, satellite echoes are affected by echoes from non-ocean surfaces such as land and islands. The standard waveform is contaminated, and the satellite observation accuracy is reduced. The standard waveforms of satellite data of the T/P series are similar. Six arcs (Appendix B) of the Jason-1 satellite from sea to land or from land to sea were selected from the study area. The echo power of each arc within 30 km from the coastline is shown in Figure 3.

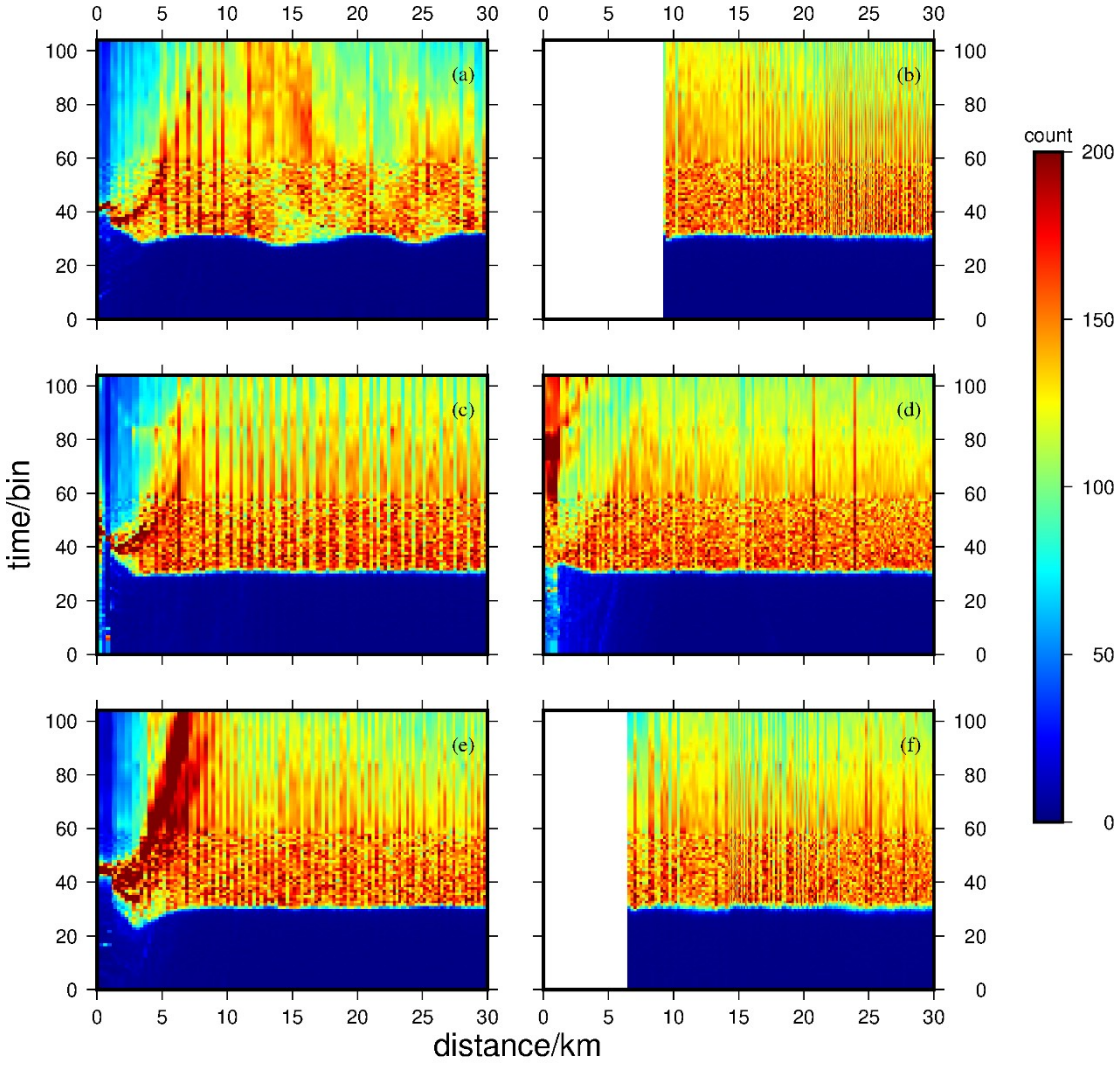

Figure 3 Echo power for each selected arc

As shown in Figure 3 (a), (c), (d) and (e), the waveforms of Janson-1 began to be contaminated approximately 10 km from the coastline. The closer the waveform is to the coastline, the more serious the waveform is contaminated and the greater the accuracy of sea level observations. There is no obvious waveform contamination of arcs 2 and 6 in cycle 18, but the two arcs only have waveform data after 9.361 km and 6.596 km from the coastline. Therefore, the tide gauge station is used to correct the SSH of SJAO2020A 10 km away from the coastline.

3.2.2 Improvement of offshore accuracy of mode

The Gaussian inverse distance weighting method is used to correct the SSH of grid points within 10 km from 24 tide stations. Then, the adjustable tensor continuous curvature spline interpolation method is used to correct all offshore grid points of SJAO2020A. The final MSS model over the Sea of Japan and its adjacent ocean (named SJAO2020) was established, as shown in Figure 4.

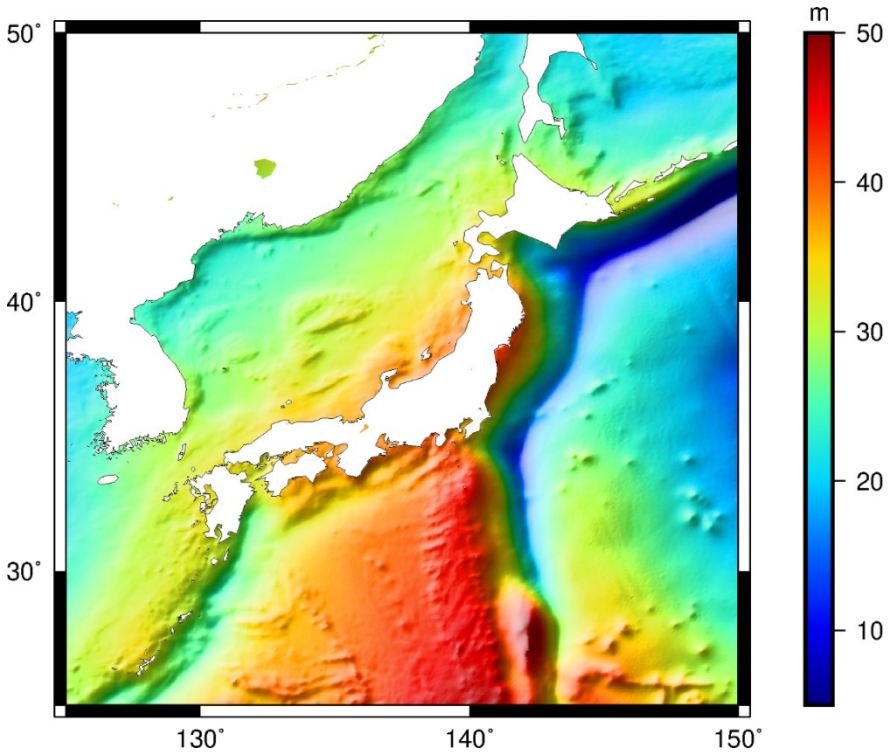

Figure 4 SJAO2020 MSS model

Figure 4 shows that the SSH change over the Sea of Japan and its adjacent ocean areas is complicated. The overall SSH of the Philippine plate is higher than that of the Pacific plate. Among them, the SSH of the Izu-Ogasawara Trench, Japan Trench and Thousand Islands Trench is low. and the lowest point is the Thousand Islands Trench, which is -2.826 m. The highest point at SSH is 52.9643 m, near the Ogasawara Islands.

To verify the offshore accuracy of SJAO2020 corrected by the tide gauge station, the SSHs of DTU18, CLS15, SJAO2020A and SJAO2020 at the position of the tide gauge station were interpolated and compared with the actual measured SSHs of the tide gauge stations. The statistical results are shown in Table 5.

Table 5 Statistics of offshore grid corrections

Tide	H_{tide}	H_{Arch}	H_{cnk}	Improvements
Ogi	38.8718	38.8348	38.8917	45.80%
Tajiri	36.6258	36.6799	36.6399	73.94%

Ito II	40.5066	40.3941	40.4708	68.17%
Kushimoto	39.6676	39.7160	39.6874	59.09%

Note: Improvement=$1-\left|H_{ssh}-H_{tide}\right|/\left|H_{Assh}-H_{tide}\right|$

In Table 5, H_{Assh} and H_{ssh} represent the SSH at the tide gauge station calculated by SJAO2020A and SJAO2020, respectively. The SSH difference between SJAO2020 and the four tide gauge stations is approximately 2 cm, which obviously improves the SSH difference between SJAO2020A and the tide station. This indicates that the Gaussian inverse distance weighting method based on tide gauge stations and the joint GNSS can effectively improve the offshore accuracy of the SJAO2020 MSS model.

3.3 Accuracy assessment of SJAO2020

To evaluate the model error of SJAO2020 at different wavelength scales and to better quantify the difference between it and DTU18, DTU15, CLS11 and WHU13, based on the mean along-track ERM data of the 1-year uninterrupted Sentinel-3B satellite in 2019, the along-track SLAs of the Sentinel-3B and SJAO2020, DTU18, DTU15, CLS11 and WHU13 models were obtained. The power spectral density (PSD) of the along-track SLA in different wavelength ranges is obtained by using the fast Fourier transform (FFT). The Sentinel-3B data used in this study are completely independent of all models, whether time or satellite ground tracks.

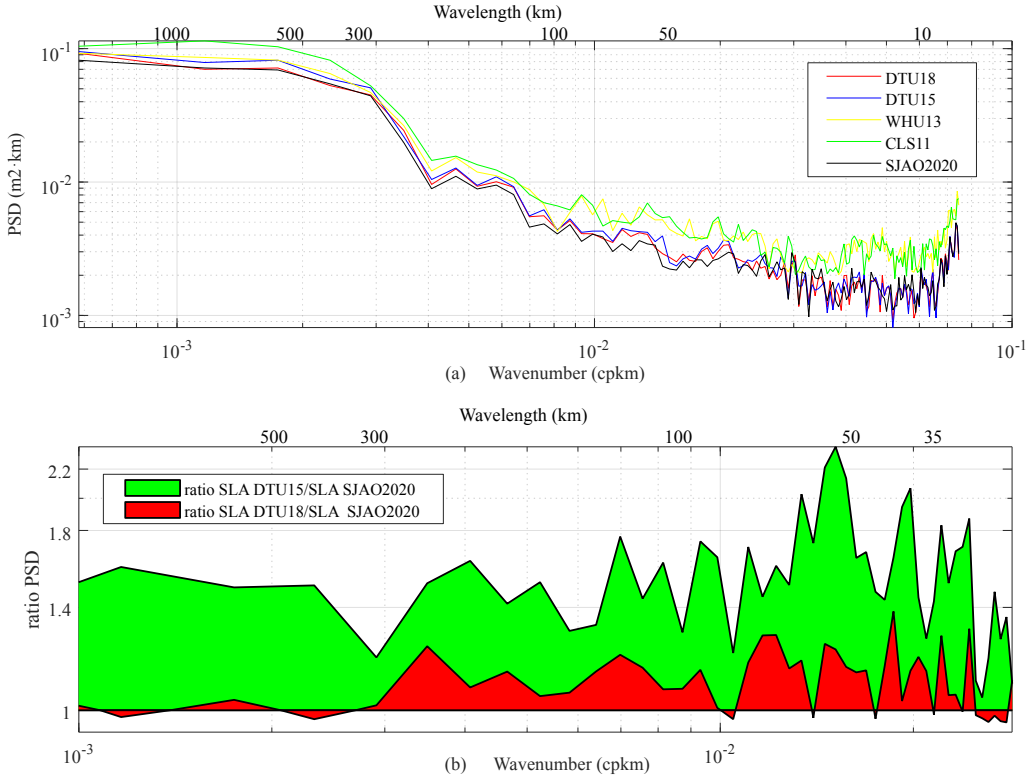

Figure 5 The PSD of the along-track SLA in different wavelength ranges. (a) Along Sentinel-3B tracks using several MSS models; (b) The ratio of spectra from panel (a)

As shown in Figure 5 (a), the error of each model is obviously different for wavelengths longer than 300 km. This is due to the independence of each model and the systematic error between each model included in the SLA time series. Among them, the systematic error between SJAO2020 and DTU18 is the smallest because the types and quantities of SSH data used by the two are the closest. The error of each model drops rapidly at wavelengths of

250~300 km. At wavelengths of 35~250 km, the SJAO2020 error is significantly improved compared to other models. In the smaller wavelength range of 12~18 km, the errors of each model have a small increase, of which satellite altimeter noise is dominant (Pujol et al., 2018). Figure 8(b) shows the ratio of the along-track PSD of DTU15 and DTU18 in Figure 8(a) to the along-track PSD of SJAO2020. Compared with DTU18 and DTU15, the SLA change of SJAO2020 is reduced by 11.76% and 59.24% in the wavelength range of 35~300 km, and the improvement is greatest when the wavelength is 66 km.

As seen from the above, satellite altimeter data are also an effective method for evaluating the MSS model. The SLA of satellite altimeter data and five models were obtained separately. Among them, the satellite altimeter data include collinear data of the T/P series, ERS-1, HY-2A and Sentinel-3B as well as GM data of Jason-2 and SARAL (Due to technical problems, the SARAL satellite drifted in repetitive periodic tracks in March 2015. Compared with historical repetitive tracks, the maximum drift amount is up to 10 km.). The root mean square error of each SLA in the wavelength range of 35 to 300 km is calculated by Chebyshev bandpass filtering. The statistical results are shown in Table 6.

Table 6 STD of the short wavelengths along-track SLA of different altimeters and using different MSS solutions (passband filtered from 35 to 300 km). (Units m)

Altimetric satellite	SJAO2020	DTU18	DTU15	WHU13	CLS11
T/P+Japan-1+Japan-2+Japan-3 (1992.12.31-2018.12.31)	0.0138	0.0186	0.0196	0.0265	0.0292
ERS-1(1992.11.227-1993.12.30)	0.0217	0.0223	0.0224	**0.0226**	**0.0222**
HY-2A(2014.04.12-2016.03.15)	0.0201	**0.0222**	**0.0228**	**0.0255**	**0.0264**
SENTINEL-3B(2018.11.27-2019.11.05)	**0.0292**	**0.0319**	**0.0320**	**0.0342**	**0.0358**
SARAL(2015.03.19-2016.07.04)	**0.0435**	**0.0443**	**0.0449**	**0.0517**	**0.0529**
Jason-2/GM(2017.07.29-2017.09.14)	**0.0414**	**0.0426**	**0.0430**	**0.0494**	**0.0497**

Note: The figures for independent data sets (not used in the MSS model) are highlighted in bold.

As shown in Table 6, the STD of the SLA given by SJAO2020 and its benchmark (T/P series) data in the wavelength range of 35 to 300 km is the smallest compared to the other four models, indicating that the model is the most stable and the data processing results are more reliable. The STD of the along-track SLA given by between HY-2A and SJAO2020 is significantly smaller than that of the other four models. This is because HY-2A data are only used in SJAO2020, indicating that the accuracy of the MSS model at the ground track of the satellite can be improved by adding more high accuracy satellite observations. Sentinel-3B, SARAL and Jason-2/GM are not used in the establishment of the SJAO2020, DTU18, DTU15, WHU13 and CLS11 models, and the STDs of the three satellite data along-track SLA are sequentially reduced. This shows that the accuracy of the SJAO2020 model is the highest. Compared with DTU15, the accuracy of DTU18 has been improved, and the accuracy of both models is better than WHU13. However, the ERS-1 along-track data are consistent with CLS11, only second to SJAO2020 and better than DTU18 DTU15 and WHU13. This may be caused by the establishment of the CLS11 model using only the GM

data of one ERS-1 satellite. The model has a strong correlation with the ERS-1 satellite.

4 Conclusions

A new MSS model named SJAO2020A with a grid of $1' \times 1'$ over the Sea of Japan and its adjacent ocean was established with a 19-year moving average method by combining satellite altimeter data from 1993 to 2018. The ERM data of all satellites are adjusted by collinear adjustment, and the temporal oceanic variability in GM data is corrected. Then, the single-satellite and multisatellite altimeter data are successively adjusted by crossover adjustment. The SJAO2020A model is obtained by using the least square collocation method. Different from the latest international MSS models CLS15 and DTU18, the measured data of the latest altimetry satellites HY-2A, Janson-3 and Sentinel-3A are also introduced into SJAO2020A. To improve the offshore accuracy of SJAO2020A, the 24 tide gauge stations and the joint GNSS along the coast of Japan are used to correct the SSH within 10 km from the coastline by using the Gaussian inverse distance weighting method. Finally, the SJAO2020 model with higher offshore accuracy is obtained. The difference between SJAO2020 and the four tide gauge stations is approximately 2 cm, and the offshore accuracy is better than that of CLS15 and DTU18.

To better quantify the differences between the models, this study obtained the PSD of the along-track SLA between Sentinel-3B and the SJAO2020, DTU18, DTU15, CLS11 and WHU13 models. The SLA change of SJAO2020 is 11.76% and 59.24% lower than that of DTU18 and DTU15 in the wavelength range of 35~300 km, respectively. Through the STD analysis of the along-track SLA between different satellite data and each model in the wavelength range of 35 to 300 km, the SJAO2020 model has the smallest error. The errors of the DTU18 and DTU15 models are smaller than those of WHU13 and CLS11, and the accuracy of the DTU18 model is slightly better than that of DTU15.

Appendix A: Data grouping based on the 19-year interval

Group	Altimeter data（cycle）
1992.12.31-2011.12.31	Topex/A（11-353）、Jason-1/A（11-249）、Jason-2/A（11-128）、Topex/B（369-479）、Jason-1/B（262-372）、ERS-1（16-27;41-51）、ERS-2（7-80）、GFO（45-215）、Envisat/A（6-89）、Envisat/B（100-111）、ERS-1/168（30-40）、CryoSat-2/LRM（14-25）
1993.12.31-2012.12.31	Topex/A（47-353）、Jason-1/A（11-249）、Jason-2/A（11-165）、Topex/B（369-479）、Jason-1/B（262-372）、ERS-1（41-51）、ERS-2（7-80）、GFO（45-215）、Envisat/A（6-89）、Envisat/B（100-111）、ERS-1/168（30-40）、Jason-1/GM（500-521）、CryoSat-2/LRM（14-37）
1994.12.31-2013.12.31	Topex/A（84-353）、Jason-1/A（11-249）、Jason-2/A（11-202）、Topex/B（369-479）、Jason-1/B（262-372）、ERS-1（41-51）、ERS-2（7-80）、GFO（45-215）、Envisat/A（6-89）、Envisat/B（100-111）、ERS-1/168（38-40）、Jason-1/GM（500-537）、CryoSat-2/LRM（14-50）
1995.12.31-2014.12.31	Topex/A（121-353）、Jason-1/A（11-249）、Jason-2/A（11-239）、Topex/B（369-479）、Jason-1/B（262-372）、SARAL（1-11）、HY-2A（67-92）、ERS-2（7-80）、GFO（45-215）、Envisat/A（6-89）、Envisat/B（100-111）、Jason-1/GM（500-537）、CryoSat-2/LRM（14-62）
1996.12.31-	Topex/A（158-353）、Jason-1/A（11-249）、Jason-2/A（11-276）、Topex/

2015.12.31	B（369-479）、Jason-1/B（262-372）、SARAL（1-21）、ERS-2（18-80）、GFO（45-215）、Envisat/A（6-89）、Envisat/B（100-111）、Jason-1/GM（500-537）、CryoSat-2/LRM（14-75）
1997.12.31-2016.12.31	Topex/A（195-353）、Jason-1/A（11-249）、Jason-2/A（11-290）、Jason-3/A（11-33）、Topex/B（369-479）、Jason-1/B（262-372）、SARAL（1-21）、HY-2A（67-117）、ERS-2（28-80）、GFO（45-215）、Envisat/A（6-89）、Envisat/B（100-111）、Jason-1/GM（500-537）、CryoSat-2/LRM（14-75）、SARAL/DP（100-104）、HY-2A/GM（118-148）
1998.12.31-2017.12.31	Topex/A（231-353）、Jason-1/A（11-249）、Jason-2/A（11-290）、Jason-3/A（11-69）、Topex/B（369-479）、Jason-1/B（262-372）、SARAL（1-21）、HY-2A（67-117）、ERS-2（38-80）、GFO（45-215）、Envisat/A（6-89）、Envisat/B（100-111）、Sentinel-3A（12-25）、Jason-1/GM（500-537）、CryoSat-2/LRM（14-101）、SARAL/DP（100-115）、HY-2A/GM（121-189）
1999.12.31-2018.12.31	Topex/A（268-353）、Jason-1/A（11-249）、Jason-2/A（11-290）、Jason-3/A（11-106）、Topex/B（369-479）、Jason-1/B（262-372）、SARAL（1-21）、HY-2A（67-117）、ERS-2（49-80）、GFO（45-215）、Envisat/A（6-89）、Envisat/B（100-111）、Sentinel-3A（13-39）、Jason-1/GM（500-537）、CryoSat-2/LRM（14-113）、SARAL/DP（100-125）、HY-2A/GM（118-189）

Appendix B: Ground tracks of Jason-1 and geographical distribution of waveform data

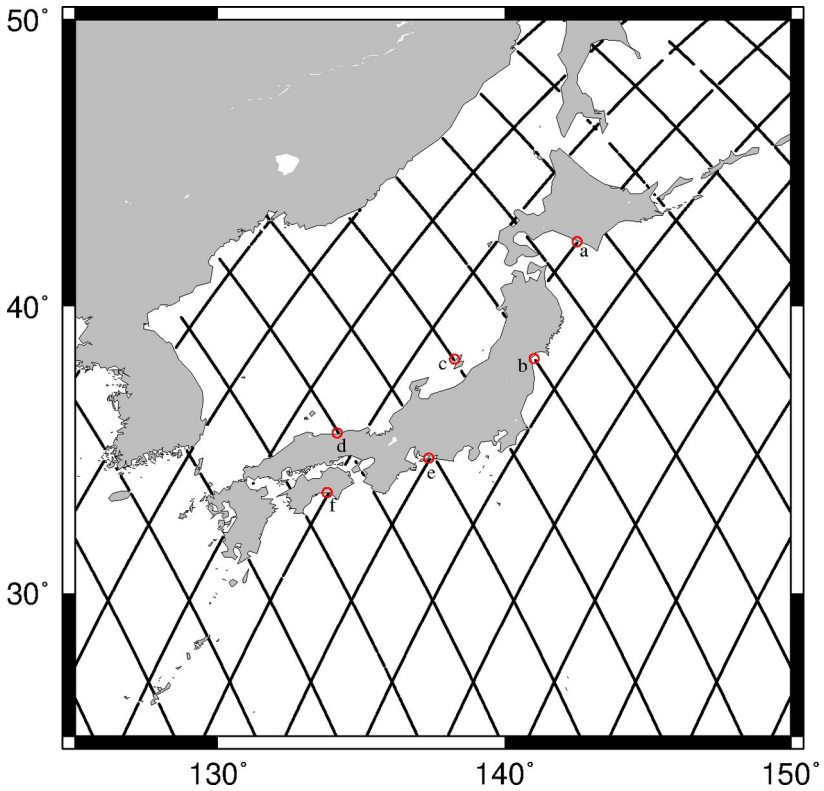

Acknowledgements

We are very grateful to AVISO+ for providing the along-track L2P products and the waveform data of Jason-1, which can be obtained by downloading freely from AVISO+ official website (ftp://ftp-access.aviso.altimetry.fr). The tide gauge records is available online (https://www.psmsl.org/) and the GPS data is available online (https://www.sonel.org). This study is supported by the National Natural Science Foundation of China (Grant Nos. 41774001, 41704015), the Special Project of Basic Science and Technology of China (Grant No. 2015FY310200), and the Autonomous and Controllable Special Project for Surveying and Mapping of China (Grant No. 816-517).

References

Andersen, O. B., & Knudsen, P. (2009). DNSC08 mean sea surface and mean dynamic topography models. *Journal of Geophysical Research*, 114(C11), C11001. https://doi.org/10.1029/2008jc005179

Andersen, O.B., Knudsen, P., & Stenseng, L., (2015). The DTU13 MSS (mean sea surface) and MDT (mean dynamic topography) from 20 years of satellite altimetry. In: Jin, S., Barzaghi, R. (Eds.), IGFS 2014. International Association of Geodesy Symposia, Springer, Cham, Switzerland, 144, 111–120. https://doi.org/10.1007/1345_ 2015_182

Andersen, O.B., Piccioni, G., Stenseng, L., & Knudsen, P. (2016). The DTU15 MSS (mean sea surface) and DTU15LAT (lowest astronomical tide) reference surface. In: Proceedings of the ESA Living Planet Symposium 2016. Prague, Czech Republik, 9–13 May 2016. https://ftp.space.dtu.dk/pub/DTU15/DOCUMENTS/MSS/DT U15MSSþLAT.pdf.

Andersen, O., Knudsen, P., & Stenseng, L. (2018). A new DTU18 MSS mean sea surface – improvement from SAR altimetry. 172. Abstract from 25 years of progress in radar altimetry symposium, 24-26, September 2018, Ponta Delgada, São Miguel Island Azores Archipelago, Portugal.

Basic, T., & Rapp, R. H. (1992) Oceanwide prediction of gravity anomalies and sea surface heights using Geos-3, Seasat, and Geosat altimeter data and ETOPO5U bathymetric data. Columbus: The Ohio State University. OSU Report, 416, pp.1-89.

Bird, P. (2003). An updated digital model of plate boundaries. *Geochemistry Geophysics Geosystems*, 4(3), 1027. https://doi.org/10.1029/2001GC000252

CNES. (2017). Along-track level-2+ (L2P) SLA product handbook. SALP-MU-P-EA-23150-CLS, Issue1.0.https://www.aviso.altimetry.fr/fileadmin/documents/data/tools/ hdbkL2P_all_missions_except_S3.pdf.

Dufau, C., Orstynowicz, M., Dibarboure, G., Morrow, R., & La Traon, P.-Y. (2016). Mesoscale resolution capability of altimetry: Present & future. *Journal of Geophysical Research: Oceans*, 121(7), 4910–4927. https://doi.org/10.1002/2015jc010904

Guo, J. Y., Gao, Y. G., Hwang, C. W., & Sun, J. L. (2010). A multi-subwaveform parametric retracker of the radar satellite altimetric waveform and recovery of gravity anomalies over coastal oceans. *Science China Earth Sciences*, 53(4), 610–616. https://doi.org/10.1007/s11430-009-0171-3

Guo, J., Wang, J., Hu, Z., Hwang, C., Chen, C., & Gao, Y. (2015). Temporal-spatial variations of sea level over Chinese seas derived from altimeter data of TOPEX/Poseidon, Jason-1 and Jason-2 from 1993 to 2012. *Chinese Journal of Geophysics*, 58(9), 3103-3120. https://doi.org/10.6038/cjg20150908

Guo, J., Wang, J., Hu, Z., Liu, X., Kong, Q., & Zhao, C. (2016) Vertical land movement over China coasts determined by tide gauge and satellite altimetric data. *Arabian Journal of Geosciences*, 9(3), 168. https://doi.org/10.1007/s12517-015-2219-3

Holgate, S. J., Matthews, A., Woodworth, P. L., Rickards, L. J., Tamisiea, M. E., Bradshaw, E., et al. (2013). New data systems and products at the permanent service for mean sea level. *Journal of Coastal Research*, 29(3), 493-504. https://doi.org/10.2307/23486334

Hassani, H. (2007). Singular spectrum analysis: methodology and comparison. *Journal of Data Science*, 5(2), 239-257.

Hernandez, F., & Schaeffer, P. (2001). The CLS01 Mean Sea Surface: a Validation with the GSFC00.1 Surface. CLS Ramonville St Agne, France.

Huang, M. T., Wang, R., Zhai, G. J., & Ouyang, Y. Z. (2007). Integrated data processing for multi-satellite missions and recovery of marine gravity field. *Geomatics and Information Science of Wuhan University*, 32(11), 988-993. https://doi.org/10.13203/ j.whugis2007.11.010

Ishii, M., Kimoto, M., Sakamoto, K., & Iwasaki, S.-I. (2006). Steric sea level changes estimated from historical ocean subsurface temperature and salinity analyses. *Journal of Oceanography*, 62(2), 155-170. https://doi.org/10.1007/s10872-006-0041-y

Jiang, W., Li, J., & Wang, Z. (2002). Determination of global mean sea surface WHU2000 using multi-satellite altimetric data. *Chinese Science Bulletin*, 47(19), 1664–1668. https://doi.org/10.1007/bf03184119

Jin, T. Y., Li, J. C., Jiang, W. P., & Wang, Z. T. (2011). The new generation of global mean sea surface height model based on multi-altimetric data. *Acta Geodaetica et Cartographica Sinica*, 40 (6), 723–729. https://doi.org/10.1007/s11769-011-0446-4

Jin, T. Y., Li, J. C., & Jiang, W. P. (2016). The global mean sea surface model WHU2013. *Geodesy and Geodynamics*, 7(3), 202–209. https://doi.org/10.1016/j.geog.2016.04.006

Marsh, J. G., Koblinsky, C. J., Zwally, H. J., Brenner, A. C., & Beckley, B. D. (1992). A global mean sea surface based upon GEOS 3 and Seasat altimeter data. *Journal of Geophysical Research*, 97(B4), 4915-4921. https://doi.org/10.1029/91jb03153

Menéndez, M., & Woodworth, P. L. (2010). Changes in extreme high water levels based on a quasi-global tide-gauge data set. *Journal of Geophysical Research*, 115(C10), C10011. https://doi.org/10.1029/2009jc005997

Pujol, M.-I., Schaeffer, P., Faugère, Y., Raynal, M., Dibarboure, G., & Picot, N. (2018). Gauging the improvement of recent mean sea surface models: a new approach for identifying and quantifying their errors. Journal of Geophysical Research: Oceans, 123(8), 5889–5911. https://doi.org/10.1029/2017jc013503

Rummel, R. (1993). Principle of satellite altimetry and elimination of radial orbit errors. Satellite altimetry in geodesy and oceanography. Springer, Berlin, Heidelberg, pp. 190-241.

Santamaría-Gómez, A., Gravelle, M., Dangendorf, S., Marcos, M., Spada, G., & Wöppelmann, G. (2017). Uncertainty of the 20th century sea-level rise due to vertical land motion errors. *Earth and Planetary Science Letters*, 473, 24-32. https://doi.org/10.1016/j.epsl.2017.05.038

Santamaría-Gómez, A., Gravelle, M., Collilieux, X., Guichard, M., Míguez, B. M., Tiphaneau, P., et al. (2012). Mitigating the effects of vertical land motion in tide gauge records using state-of-the-art GPS velocity field. *Global and Planetary Change*, 98–99, 6–17. https://doi.org/10.1016/j.gloplacha.2012.07.007

Schaeffer, P., Ollivier, A., Faugere, Y., Bronner, E., & Picot, N. (2010). The new CNES CLS 2010 mean sea surface. In: Oral Presentation at OSTST Meeting, Lisbon, Portugal, pp. 21–22. October 2010. https://www.aviso.altimetry.fr/fileadmin/documents/ OSTST/2010/oral/Schaeffer.pdf.

Schaeffer, P., Faugére, Y., Legeais, J. F., Ollivier, A., Guinle, T., & Picot, N. (2012). The CNES_CLS11 Global Mean Sea Surface Computed from 16 Years of Satellite Altimeter Data. *Marine Geodesy*, 35(sup1), 3–19. https://doi.org/10.1080/01490419.2012.718231

Shen, Y., Guo, J., Liu, X., Kong, Q., Guo, L., & Li, W. (2018). Long-term prediction of polar motion using a combined SSA and ARMA model. *Journal of Geodesy*, 92(3), 333-343. https://doi.org/10.1007/s00190-017-1065-3

Small, H. (1992). A comparison of techniques for the gridding of satellite altimeter data. Columbus: The Ohio State University.

Smith, W. H. F., & Wessel, P. (1990). Gridding with continuous curvature splines in tension, *Geophysics*, 55(3), 293–305. https://doi.org/10.1190/1.1442837

Sui, X., Zhang, R., Wu, F., Li, Y., & Wan, X. (2017). Sea surface height measuring using InSAR altimeter.

Geodesy and Geodynamics, 8(4), 278–284. https://doi.org/10.1016/j.geog.2017.03.005

Wagner, C. A. (1985). Radial variations of a satellite orbit due to gravitational errors: Implications for satellite altimetry. *Journal of Geophysical Research: Solid Earth*, 90(B4), 3027-3036. https://doi.org/10.1029/jb090ib04p03027

Yi, Y. (1995). Determination of gridded mean sea surface from Topex. ERS-1 and Geosat altimeter data. Columbus: The Ohio State University.

Yuan, J., Guo, J., Niu, Y., Zhu, C., Li, Z., & Liu, X. (2020a). Denoising Effect of Jason-1 Altimeter Waveforms with Singular Spectrum Analysis: A Case Study of Modelling Mean Sea Surface Height over South China Sea. Journal of Marine Science and Engineering, 8(6), 426. https://doi.org/10.3390/jmse8060426

Yuan, J., Guo, J., Liu, X., Zhu, C., Niu, Y., Li, Z., et al. (2020b). Mean sea surface model over China seas and its adjacent ocean established with the 19-year moving average method from multi-satellite altimeter data. *Continental Shelf Research*, 192(1), 104009. https://doi.org/10.1016/j.csr.2019.104009

Zhu, C., Guo, J., Hwang, C., Gao, J., Yuan, J., & Liu, X. (2019). How HY-2A/GM altimeter performs in marine gravity derivation: assessment in the South China Sea. *Geophysical Journal International*, 219(2), 1056–1064. https://doi.org/10.1093/gji/ggz330.zi

Zhu, C., Guo, J., Gao, J., Liu, X., Hwang, C., Yu, S., et al. (2020).Marine gravity determined from multi-satellite-GM/ERM altimeter data over the South China Sea: SCSGA V1.0. *Journal of Geodesy*, 94(5), 50. https://doi.org/10.1007/s00190-020-01378-4